C. R. Chimie 21 (2018) 182–193

Contents lists available at ScienceDirect

Comptes Rendus Chimie

www.sciencedirect.com

Full paper/Mémoire

# Influence of the formulation of catalysts deposited on cordierite monoliths for acetic acid oxidation

## *Influence de la composition des catalyseurs déposés sur des monolithes en cordiérite pour l'oxydation de l'acide acétique*

Henri-Joël Sedjame [a], Rachid Brahmi [b], Gwendoline Lafaye [a], Jacques Barbier Jr. [a], Céline Fontaine [a, *]

[a] Université de Poitiers, CNRS UMR 7285 IC2MP, 4, rue Michel-Brunet, 86073 Poitiers cedex, France
[b] UCD, Laboratoire de catalyse et de corrosion des matériaux, Faculté des sciences, 24000 El Jadida, Morocco

ARTICLE INFO

*Article history:*
Received 8 March 2017
Accepted 24 August 2017
Available online 9 October 2017

*Keywords:*
Heterogeneous catalysis
Acetic acid
Catalytic oxidation
Monoliths
Platinum
Basicity
Redox chemistry

ABSTRACT

Monolithic catalysts are prepared by washcoating cordierite monoliths with different sols ($Pt/Al_2O_3$, $Pt/CeO_2$, $Pt/ZrO_2$, $Pt/Al_2O_3–CeO_2$, $Pt/Al_2O_3–ZrO_2$, and $Pt/CeO_2–ZrO_2$). These sols are prepared by a sol–gel process and characterized by specific surface area ($S_{BET}$), inductively coupled plasma, hydrogen chemisorption, high-resolution transmission electron microscopy, field emission scanning electron microscopy, oxygen storage capacity, X-ray diffraction, temperature-programmed reduction, $CO_2$ chemisorption, and the model reaction of 3,3-dimethylbutene isomerization. The catalytic performances of the monolithic catalysts are then evaluated for the acetic acid oxidation. The nature of catalyst coating has been found to influence the adherence with the cordierite monolith and the presence of cerium in the catalyst appears to increase the adherence of the latter. $Pt/CeO_2$, $Pt/Al_2O_3–CeO_2$, and $Pt/CeO_2–ZrO_2$ are found to be the most reducible catalysts (oxygen storage capacity and temperature-programmed reduction) and to have the lowest acidities (3,3-dimethylbutene isomerization). $CO_2$ chemisorption shows that these catalysts possess a good basicity. From the relation established between the catalytic activity and the redox and acid–base properties it has been concluded that the reducibility is the key factor for a good catalytic activity although the basicity has a significant influence on the catalytic performance.



*Mots clés:*
Catalyse hétérogène
Acide acétique
Oxydation catalytique
Monolithes

RÉSUMÉ

L'oxydation catalytique de l'acide acétique a été étudiée sur des catalyseurs monolithiques enduits de divers matériaux à base de platine. Les matériaux utilisés sont $Pt/Al_2O_3$, $Pt/CeO_2$, $Pt/ZrO_2$, $Pt/Al_2O_3–CeO_2$, $Pt/Al_2O_3–ZrO_2$ et $Pt/CeO_2–ZrO_2$. Les solutions d'enduction ont été préparées par la méthode sol–gel et les matériaux ont, dans un premier temps, été caractérisés par mesure de surface spécifique ($S_{BET}$), analyse

* Corresponding author.
*E-mail address:* celine.fontaine@univ-poitiers.fr (C. Fontaine).

http://dx.doi.org/10.1016/j.crci.2017.08.004

Platine
Basicité
Oxydo-réduction

élémentaire (ICP), chimisorptions d'hydrogène et de $CO_2$, microscopie (HRTEM et FESEM), mesure des capacités de stockage de l'oxygène (OSC), diffraction des rayons X (XRD), réduction en température programmée (TPR) et la réaction modèle d'isomérisation du 3,3-diméthylbutène. Les performances catalytiques des solides ont ensuite été évaluées pour la réaction d'oxydation de l'acide acétique. Il semble que la nature de la solution d'enduction influence l'adhérence aux parois du monolithe. Ainsi la cérine apparait comme le support qui adhère le mieux au monolithe et la zircone celui qui adhère la moins bien. Les caractérisations semblent montrer que $Pt/CeO_2$, $Pt/Al_2O_3–CeO_2$ et $Pt/CeO_2–ZrO_2$ sont les matériaux les plus réductibles (OSC et TPR), ainsi que la plus faible acidité (isomérisation du 3,3-diméthylbutène). La chimisorption de $CO_2$ indique que ces solides présentent une basicité intéressante. À partir de la relation entre l'activité catalytique et les propriétés redox et acido-basiques, il semble que la réductibilité des matériaux soit le paramètre clé afin d'obtenir une bonne activité catalytique, bien que la basicité ait également une influence significative sur les performances des matériaux.



## 1. Introduction

Volatile organic compounds (VOCs) are defined as any organic compound whose vapor pressure is at least 10 Pa at 20 °C or having a corresponding volatility under the particular conditions of use. Emissions of these compounds from natural-gas-fed engines, wastewater treatment plants, food processing plants, landfills, composting of different solid wastes, and animal feeding operations [1–5] are known to be a problem because many of these compounds are malodorous and dangerous for human health and nature [6–10]. It is the case of some organic acids such as formic and acetic acids, which are known to be important constituents of the “natural” atmosphere both in gas phase and hydrometeors [11,12]. These acids play a major role in the rainwater acidity observed in some parts of the world [11,13].

To reduce these emissions several techniques have been developed such as incineration, irradiation, biotreatment, adsorption, absorption, condensation, and membrane techniques [14]. Among these techniques, catalytic oxidation appears to be the most effective for the removal of low concentrations of VOCs [15]. In fact, catalytic oxidation decreases the oxidation temperature compared to thermal methods. The energy consumed is thus lowered.

Organic acids are also obtained as byproducts for VOC oxidation [16]. Ali et al. have shown that among several organic acids, acetic acid is the most difficult to oxidize [2]. In fact, this refractory aspect to oxidize acetic acid is widely mentioned in the literature even if most of the studies deal with its degradation in water [16,17]. Oliviero et al. [16] have noted that acetic acid obtained as a byproduct in phenol catalytic wet air oxidation is one of the most refractory molecules. Acetic acid oxidation is, therefore, regarded as a rate-determining step in the oxidation reaction of various organic compounds. However, the elimination of acetic acid in the gas phase is only barely studied, even if its volatility is relatively high (saturation vapor pressure = 1.5 kPa at 20 °C). As a consequence, only a few studies can be found in the literature [2]. To our knowledge, only Ali et al. reported a catalytic oxidation of acetic acid over copper supported on alumina catalysts. On the contrary, numerous catalytic systems such as zeolites [18–21], mixed oxide catalysts [22–26], or noble metal catalysts [27–32] are proposed to be efficient for the removal of other VOC classes. In gas phase catalytic reactions, these catalysts are often used in a powder form in a fixed bed reactor for laboratory research. Therefore, for almost all industrial applications, the catalysts used are structural shaped materials. Different forms of carriers have been studied such as monoliths, foams, pellets, and spheres [33–39].

Among the shaped carriers developed and used as catacomb monoliths are the most successful because of their advantages compared to extrudates or pellets (used in packed bed reactor) [14,40]. In fact, monoliths are unibody structures composed of interconnected repeating cells or channels, which lead to a large open frontal area resulting in very little resistance to flow and hence low pressure drop. Moreover, monolithic supports allow a better thermal shock, attrition resistance, uniform flow distribution and mass/heat transfer conditions, and shorter diffusion length [14,40]. Although in the past catalytic converters are commonly used in the vehicle exhausts systems, nowadays the monolith is the favorite support for almost all environmental applications where high flow rates and low pressure are required. This is why it seems to be very interesting to study monolithic-shaped catalysts in our experimental conditions to compare the results with the powder catalysts. Because the cordierite monolith possesses a low surface area (0.5–0.7 $m^2\ g^{-1}$), another catalytically active and high-surface area material is applied on the monolith walls by a washcoating procedure [39,41,42]. Although a few years ago γ alumina was practically the only support used for the washcoating of monoliths, today several sol–gel procedures that allow the deposition of other supports, which present interesting properties for oxidation (acid–base, redox, high oxygen storage, mobility, and so forth), are being developed.

This article is focused on the catalytic oxidation of acetic acid using monolithic catalysts. The cordierite monoliths have been coated with different platinum-supported

catalysts prepared by sol–gel method and known for their acid–base and redox properties. These catalysts are Pt/$Al_2O_3$, Pt/$ZrO_2$, Pt/$CeO_2$, Pt/$Al_2O_3$–$CeO_2$, Pt/$Al_2O_3$–$ZrO_2$ and Pt/$CeO_2$–$ZrO_2$. Characterizations have been made to determine the redox and acid–base properties of the synthesized catalysts. The catalytic performances of the catalysts have then been evaluated for the acetic acid oxidation and to explore a possible correlation between the catalytic activity and the redox and acid–base properties.

## 2. Experimental section

### 2.1. Preparation of monolithic catalysts

First, the commercial cordierite ($Al_3Mg_2AlSi_5O_{18}$) honeycomb monoliths provided by CTI company (Salindres, France) with a cell density of 200 cpsi, a wall thickness of 0.25 mm, a cell spacing of 1.43 mm, square channels, 25 mm of diameter, and 30 mm length were sliced in sections of 5 mm to fit the catalytic reactor.

The monolith catalysts are prepared in four steps as detailed in the following paragraphs: pretreatment of the cordierite monoliths, preparation of the washcoating solution, washcoating, and activation of the material.

The monoliths must be pretreated to remove soluble impurities and to roughen the surface prior the coating. They are immersed in nitric acid (65%) at room temperature for 1 h and then washed with ultrapure water. Before drying in a muffle furnace at 300 °C in air for 1 h, the monoliths are superficially dried with compressed air.

The washcoating sols are prepared by sol–gel method. The desired amounts of aluminum ($Al(NO_3)\cdot 9H_2O$, Aldrich, ≥98%), zirconium ($ZrO(NO_3)_2\cdot 9H_2O$, Aldrich, 99%), and/or cerium ($Ce(NO_3)_3\cdot 6H_2O$, Aldrich, 99%) are separately dissolved in absolute ethanol and mixed together to get the desired molar ratio of Al:Zr, Al:Ce, and Ce:Zr. A volume of ultrapure water, representing 5 vol % of ethanol, was added to the mixture. The solution was then stirred and heated at 80 °C together with a precursor salt of platinum ($Pt(NH_3)_4(OH)_2$, Alfa Aesar) added dropwise to obtain 0.5 wt % of platinum. After the formation of the desired sols, the stirring is stopped and the solution is cooled at 30 °C. A portion of all the sols was kept for catalyst characterization.

The washcoating is carried out by immersing the monolith in the prepared sol between 40 and 50 °C for 1 h. The unclogging of the channels is performed under a weak compressed air flow. Then, the prepared sols and the washcoated monoliths are allowed to mature overnight at room temperature before thermal activation. Because it is difficult to characterize monolithic catalysts without breaking or crushing them, the characterizations presented in this article are the characterizations of the prepared sols, explaining why they are submitted to the same thermal treatments as the corresponding monoliths.

The activation of the resulting powders and the monolithic catalysts consists in a calcination followed by a reduction. The slow calcination is carried out from room temperature to 500 °C (1 °C $min^{-1}$, 2 h) under air to avoid cracking of the washcoat solution. The reduction is carried out at 300 °C (10 °C $min^{-1}$) under hydrogen flow (60 mL $min^{-1}$) for 3 h.

### 2.2. Characterization

#### 2.2.1. Morphological and chemical analysis

The BET specific surface areas were measured by nitrogen physisorption at −195.8 °C using a Micromeritics Tristar apparatus. Samples were first degassed at 250 °C under high vacuum (0.1–0.2 mbar) overnight. Platinum loading was measured by inductively coupled plasma using a Perkin–Elmer Optima 2000 DV apparatus. The metal dispersion is measured by hydrogen chemisorption in a chromatographic microreactor at room temperature for alumina- and zirconia-based catalysts and at −85 °C for the catalysts containing ceria to avoid $H_2$ spillover over $CeO_2$ and/or reduction of the support. Hydrogen pulses (0.25 mL) were regularly injected after reduction under $H_2$ (300 °C, 1 h).

#### 2.2.2. Field emission scanning electron microscopy analysis

Field emission scanning electron microscopy (FESEM) measurements are performed on a Jeol JL 5600LV equipped with a tungsten filament. Samples are pretreated before analysis.

#### 2.2.3. X-ray diffraction analysis

Diffractograms and crystallite size are obtained by X-ray diffraction (XRD) using a PANalytical Empyrean θ–θ diffractometer using a Cu Kα radiation ($\lambda_{K\alpha}$ = 1.54186 Å) and equipped with a linear detector Xcelerator. The following conditions were used: dwell time 180 s, step 0.05°, and constant divergence slit 0.5°. The average crystallite size ($d$) was calculated using Scherrer's equation: $d = K\lambda_{K\alpha}/\beta_c \cos\theta$ with $\beta_c = (\beta^2 - \beta_0^2)^{1/2}$, where β (in rad) is the half-maximum line breadth of the analyzed material, $\beta_0$ (in rad) is the half-maximum line breadth of a perfectly well-crystallized $LaB_6$ standard, $K$ = 0.9 and θ is the Bragg angle for the diffraction peak considered.

#### 2.2.4. Temperature-programmed reduction

Before the temperature-programmed reduction (TPR), the catalysts were first pretreated in situ under $O_2$ for 30 min at 400 °C and cooled down to 100 °C. The TPR experiments were performed with a 1.0 vol % $H_2$/Ar gas mixture. The temperature range was 50–900 °C (5 °C $min^{-1}$) and then maintained at 900 °C for 1 h. The $H_2$ consumption was measured in an AutoChem II/Micromeritics apparatus, using a thermal conductivity detector (TCD).

#### 2.2.5. Oxygen storage capacity

The oxygen storage capacity (OSC) was measured by following the oxidation of carbon monoxide in transitory regime without oxygen in the gas phase. OSC was measured at 400 °C under atmospheric pressure using a conventional setup described in a previous work [43]. The sample is continuously purged with helium (30 mL $min^{-1}$). Successive or sequential pulses (0.25 mL) of $O_2$ (air liquid, total impurities ≤5 ppm) and CO are injected every 2 min [44,45]. The OSC is calculated from the CO consumption after stabilization of the alternate pulses ($CO/O_2$) [46]. The reaction is the following: $CO_{(g)} + 1/2\ O_{2(s)} \rightarrow CO_{2(g)} + \square_{(s)}$. Such a treatment gives information about both surface and

bulk mobile oxygen species. However, under dynamic conditions, surface species are often more involved. Therefore, OSC experiments were also carried out by reoxidizing the samples with $O_2$ pulses. Then pulses of CO and $O_2$ were alternatively injected to probe the amount of $O_2$ immediately available in these materials, which is supposed to be mainly involved in the catalytic process. Results are collected using a gas phase chromatograph equipped with a TCD and a Porapak Q column.

To go further in the interpretation, the number of oxygen atom layers (NL, Eq. (1)), involved in the storage process, is calculated on the basis of the theoretical number of reducible surface oxygen atoms ($OSC_{surf}$, Eq. (2)) and the OSC of metal ($OSC_{Pt}$, Eq. (3)):

$$NL = \frac{OSC_{meas} - OSC_{Pt}}{OSC_{surf}} \quad (1)$$

$$OSC_{surf} = \frac{bS}{Na^2} \quad (2)$$

$$OSC_{Pt} = \frac{Dw_{Me}}{100M_{Me}} \quad (3)$$

where $S$ is the BET surface area ($m^2\ g^{-1}$), $b$ the fraction of reducible elements (Ce) in the unit cell, $N$ the Avogadro number ($mol^{-1}$), $a$ the lattice parameter (m), $D$ the metal dispersion, $w_{Me}$ the metal loading, and $M_{Me}$ the metal molar mass. This calculation is based on the following assumptions:

- all the $Ce^{IV}$ atoms of the surface monolayer are reduced to lower oxidation state (III);
- the surface faces are (1 0 0) and contain two metal atoms and four oxygen atoms per unit surface area $a^2$ ($a$ = cubic parameter); therefore one oxygen atom out of four participates to the OSC process as indicated by Eqs. (4) and (5);
- the oxygen atoms bonded to reducible elements are the only ones participating in the OSC.

$$\xi\ CO\ (g) + CeO_2(s) \rightarrow CeO_{2-\xi}(s) + \xi\ CO_2\ (g) \quad (4)$$

$$CeO_{2-\xi}(s) + 1/2\ \xi\ O_2 \rightarrow CeO_2\ (s) \quad (5)$$

*2.2.6. Evaluation of the Brønsted acidity by 3,3-dimethylbut-1-ene isomerization*

The model reaction of 3,3-dimethylbut-1-ene (33DMB1) isomerization is known to involve exclusively the proton acid sites [47,48]. The reaction was performed in a plug flow reactor at 300 °C and at atmospheric pressure. The reactant flow was 15.2 mmol $h^{-1}$ and its partial pressure was 20 kPa. 33DMB1 was diluted in nitrogen by bubbling the gas through the liquid reactant in a saturator maintained at a temperature lower than room temperature. The samples were calcined in situ at 450 °C in air for 1 h before each experiment. The products were analyzed by on line gas chromatography equipped with a flame ionization detector (AlphaMos PR2100) and an Rtx-1 column (105 m × 0.53 mm × 3.00 μm).

*2.2.7. Evaluation of the basicity by $CO_2$ chemisorption*

$CO_2$ chemisorption measurements are carried out in a pulse chromatographic system. The catalyst (~50 mg) was first flushed with helium at 500 °C for 15 min and then cooled down to room temperature. Pulses of $CO_2$ (0.25 mL) were injected into a helium flow (30 mL $min^{-1}$) every 3 min until saturation. Results were collected on a gas phase chromatograph equipped with a TCD and a Poraplot Q column.

### 2.3. Catalytic tests

The gaseous feed used for the catalytic tests was composed of 1000 ppm of acetic acid in synthetic air ($O_2$/$N_2$/$H_2O$). Acetic acid and water were heated in two thermostated and pressurized (5 bar) saturators. Nitrogen was bubbled through these saturators and the outflow was mixed with the synthetic air. At the reactor inlet the gas stream was composed of 19.4% of $O_2$, 77.5% of $N_2$, 3% of $H_2O$, and 0.1% of VOC. Transfer lines were heated at 110 °C to avoid any condensation. Mass flow and temperature controllers were Brooks instruments 0254. The total flow rate was kept constant for all experiments (70 mL $min^{-1}$). Reactions were carried out in a tubular reactor placed in an electrical furnace equipped with a temperature programmer. A thermocouple was inserted in the reactor in contact with the monolithic catalyst to measure exactly the reaction temperature. The space velocity was 60,000 $h^{-1}$. The reaction products were analyzed by a gas chromatograph (Varian 490-GC) equipped with a TCD and two columns: a Porapak Q (PPQ) to analyze air and carbon dioxide and a CP-Sil 5CB to analyze hydrocarbons (butanol, butanal, acetic acid, and so forth). Experiments were performed by decreasing the temperature between 350 and 50 °C to avoid the large adsorption of acetic acid over the catalyst at low temperature.

## 3. Results and discussion

### 3.1. Characterization

As mentioned before, the characterization techniques available did not allow to study the monolith without destroying it. This is why it was decided that some of the characteristics would be determined using the dried sols in powder form before their washcoating. The monolithic catalysts should have the same properties as the corresponding powder catalysts ($Pt/Al_2O_3$, $Pt/ZrO_2$, $Pt/CeO_2$, $Pt/Al_2O_3–ZrO_2$, $Pt/Al_2O_3–CeO_2$ and $Pt/CeO_2–ZrO_2$).

*3.1.1. Morphological and chemical analysis*

The abbreviations used for the catalysts in this article are listed in Table 1.

Table 1 shows the morphological and chemical characteristics of the powder catalysts and also the weight of the layer coated for each monolith. It can be noted that the adherence of the washcoat on cordierite monoliths is more or less facilitated by the nature of the catalyst coating. In

**Table 1**
Catalysts, chemical, and morphological data.

| Catalyst coating | Bare monolith weight (g) | Coated layer weight | | %Pt (wt %) | Surface Area $S_{BET}$ ($m^2\ g^{-1}$) | Dispersion (%) | Abbreviations |
|---|---|---|---|---|---|---|---|
| | | (mg) | (%) | | | | |
| $Pt/Al_2O_3$ | 1.60 | 117.8[a] | 7.4 | 0.24 | 120 | 20 | Pt/Al |
| $Pt/CeO_2$ | 1.61 | 325.5[b] | 20.2 | 0.41 | 89 | 50 | Pt/Ce |
| $Pt/ZrO_2$ | 1.76 | 104.9[a] | 6.0 | 0.56 | 13 | 6 | Pt/Zr |
| $Pt/Al_2O_3–CeO_2$ | 1.72 | 341.7[c] | 19.8 | 0.34 | 95 | 12 | Pt/AlCe |
| $Pt/Al_2O_3–ZrO_2$ | 1.56 | 165.7[c] | 10.6 | 0.43 | 85 | 11 | Pt/AlZr |
| $Pt/CeO_2–ZrO_2$ | 1.74 | 138.1[a] | 7.9 | 0.49 | 74 | 43 | Pt/CeZr |

Abbreviations: Al stands for $Al_2O_3$, Ce for $CeO_2$, Zr for $ZrO_2$.
[a] After the third washcoat.
[b] After the first washcoat.
[c] After the second washcoat.

fact, Pt/Ce appears to be the catalyst that has the best adherence to the cordierite monolith because the coated layer weight reaches 20.2% after the first washcoat. On the contrary, Pt/Zr exhibits the lowest adherence. Actually, after the third washcoat, the coated layer weight was only 6.0%. The presence of cerium in $Pt/Al_2O_3–CeO_2$ and $Pt/CeO_2–ZrO_2$ improves the adherence of the slurries Pt/Al and Pt/Zr. Indeed, the coated layer weight increases from 7.4% to 19.8% when the slurry used is Pt/AlCe instead of Pt/Al, for example. Generally, the platinum loadings determined by inductively coupled plasma are not far from the desired loading (0.5 wt %) except for the Pt/Al catalyst. In our case, the relatively low dispersions observed can be due to an encapsulation phenomenon occurred during the preparation of the washcoating solutions. Almost all powder catalysts exhibit a high-surface area, except Pt/Z, which has a specific surface area of 13 $m^2\ g^{-1}$. Pt/Al is the catalyst that exhibits the higher surface area.

### 3.1.2. FESEM analysis

FESEM images of corresponding monolithic catalysts Pt/Ce, Pt/AlCe, and Pt/CeZr are presented in Fig. 1(a)–(c),

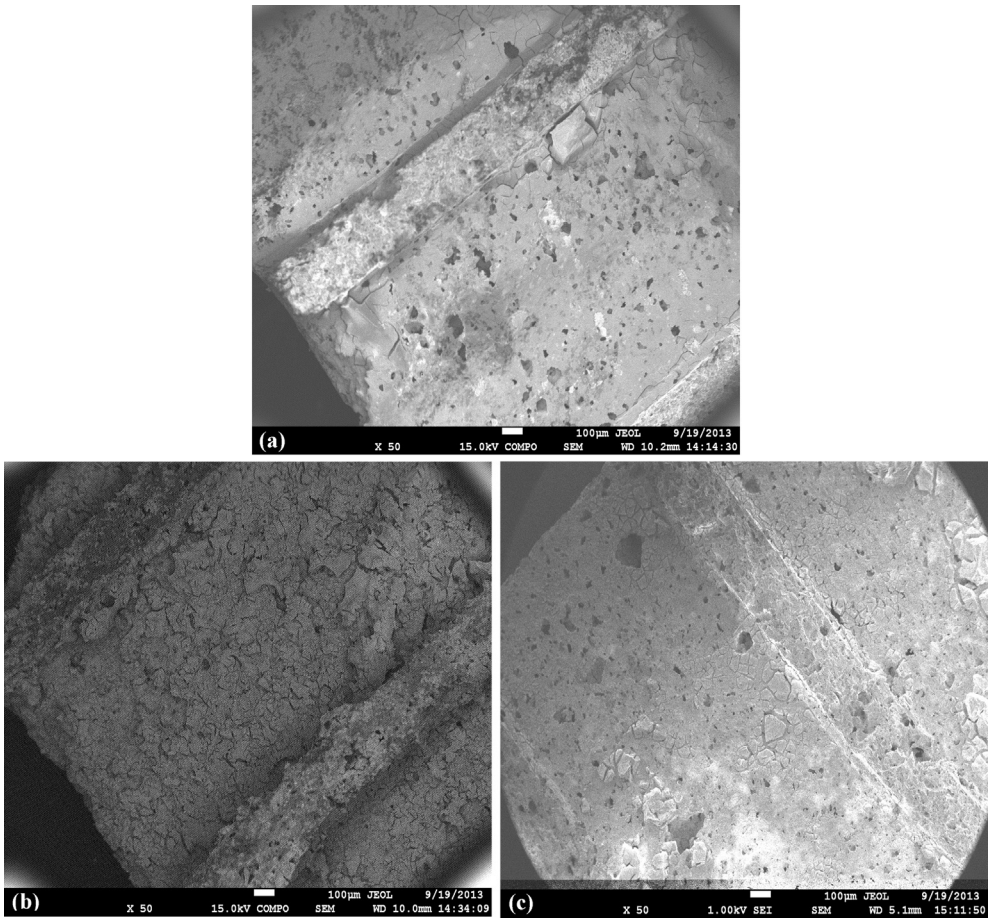


**Fig. 1.** FESEM images of the monolithic catalysts (a) $Pt/CeO_2$, (b) $Pt/Al_2O_3–CeO_2$, and (c) $Pt/CeO_2–ZrO_2$.

respectively. It can be observed that the coated layer seems to be more important on Pt/AlCe than on Pt/Ce and Pt/CeZr catalysts. In fact, Fig. 1(b) shows a thick and rough catalyst layer on the wall on the monolith whereas for Pt/Ce and Pt/CeZr catalysts, the layer coated is thinner. This observation is in agreement with the results obtained for the coated layer weight (Table 1). Nevertheless the coating is more or less homogeneous for all the analyzed samples.

### 3.1.3. XRD analysis

XRD patterns of the powder catalysts used for the monolith washcoating are reported in Fig. 2. Pt/Al exhibits an amorphous phase whereas Pt/Ce and Pt/Zr present crystallized phases with well-defined diffraction peaks. In fact Pt/Ce shows typical crystallized ceria patterns in the following region of 2θ values = 28.8°, 32.96°, 48.86°, 56.56°, 58.46°, 77.61°, 79.07°, 88.41°, and 94.73° (Fig. 2(a)). On the XRD pattern of Pt/Zr, the zirconia formation is indicated by peaks at 2θ = 30.23°, 34.65°, 35.24°, 43.03°, 53.90°, 59.39°, 60.16°, 62.86°, 73.11°, 74.51°, 81.79°, 82.47°, 83.85°, and 96.27° corresponding to the reticular planes of tetragonal $ZrO_2$ (Fig. 2(b)). Pt/Al and the platinum catalyst supported on the mixed oxide $Al_2O_3$–$ZrO_2$ have amorphous structures (Fig. 2(b)). Crystallized ceria is also observed for Pt/AlCe and Pt/CeZr catalysts. The shift toward higher angles with regard to Pt/Ce observed in Fig. 2(c) for the platinum catalyst Pt/CeZr is probably because of the formation of a solid solution.

The crystallite size and the lattice parameter of ceria were determined for the catalysts containing crystallized ceria and the results are reported in Table 2. Pt/Ce catalyst exhibits the higher ceria crystallite size (7.16 nm) and lattice parameter (5.41 Å). The ceria crystallite sizes obtained for Pt/AlCe and Pt/CeZr are 2.31 and 4.86 nm, respectively, and the corresponding lattice parameters are 5.34 and 5.35 Å. The decrease in the lattice parameters of these catalysts in comparison to Pt/Ce can be because of an insertion of $Zr^{4+}$ or $Al^{3+}$ into $CeO_2$ cubic phase resulting in the formation of solid solutions. The shift in the XRD peaks of Pt/CeZr toward higher angles with regard to Pt/Ce (Fig. 2(c)) can also be interpreted as a lattice shrink because of partial substitution of $Ce^{4+}$ (0.097 nm) by $Zr^{4+}$ (0.084 nm) [49].

### 3.1.4. TPR analysis

Fig. 3 presents the hydrogen consumption as a function of the temperature for the platinum catalysts used to coat the monolith.

The peak for Pt/Al sample at ~694 °C could be attributed to the reduction of the Pt-oxide species [50,51]. The reduction occurs at high temperature due to the low platinum loading. In fact Shyu and Otto [52] have shown that for the samples with high Pt loading (~10 wt %) this reduction occurs at lower temperature and was moved to higher temperatures with the decrease in the platinum content.

The TPR profile of Pt/Ce shows a first strong peak, which reaches its maximum at ~190 °C with a shoulder at ~255 °C and a second large and small peak between 350 and 650 °C. The first peak and its shoulder could be associated with the reduction of Pt-oxide species and the ceria surface shell. The second peak could be due to the formation of

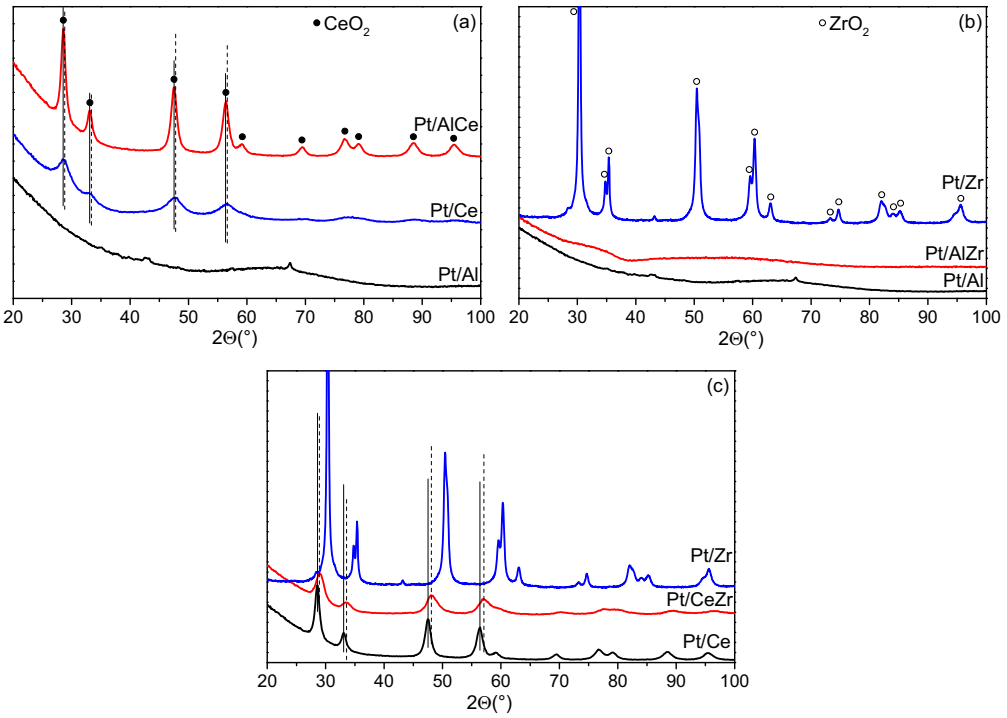


**Fig. 2.** XRD patterns of the synthesized platinum catalysts. (a) Pt supported on $Al_2O_3$ and/or $CeO_2$, (b) Pt supported on $Al_2O_3$ and/or $ZrO_2$, and (c) Pt supported on $CeO_2$ and/or $ZrO_2$.

**Table 2**
Crystallite size and lattice parameter determined by XRD measurements. OSCs and NLs determined by $CO-O_2$ chemisorption.

| Catalysts | $d$ (nm) | $a$ (Å) | $OSC_{meas}$ | $OSC_{Pt}$ | OSC | $OSC_{surf}$ | NL |
|---|---|---|---|---|---|---|---|
| Pt/Al | – | – | 22 | 2.49 | 20 | 0 | – |
| Pt/AlZr | – | – | 22 | 2.42 | 20 | 0 | – |
| Pt/Zr | – | – | 46 | 1.99 | 44 | 0 | – |
| Pt/Ce | 7.16 | 5.41 | 396 | 10.5 | 385 | 502 | 0.77 |
| Pt/AlCe | 2.31 | 5.34 | 328 | 2.1 | 326 | 200 | 1.63 |
| Pt/CeZr | 4.86 | 5.35 | 609 | 10.8 | 598 | 195 | 3.06 |

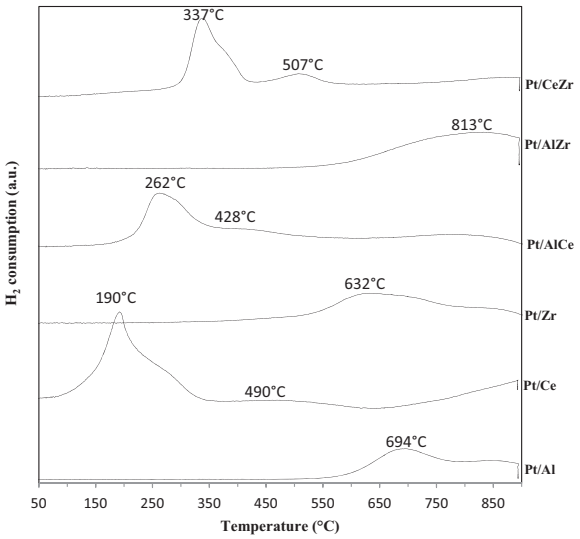


**Fig. 3.** TPR patterns of the synthesized platinum catalysts.

nonstoichiometric cerium oxides ($CeO_x$ with $x$ ranging from 1.9 to 1.7) [52,53].

The TPR profile of Pt/Z exhibits a broad peak, which reaches its maximum at 632 °C. This temperature is closer to that of $ZrO_2$ support than that of platinum-promoted $ZrO_2$. This result suggests that the promoting effect of the metal is lowered probably because of the low metallic dispersion (Table 1). The reduction peak observed could therefore be attributed to the Pt-oxide reduction and to $ZrO_2$ reduction.

The presence of cerium in both Pt/AlCe and Pt/CeZr catalysts leads to lower reduction temperature in comparison with Pt/Al and Pt/Zr, respectively. Similarly to Pt/Ce, the TPR profile of Pt/AlCe first shows an overlapped peak at 262 °C corresponding to the reduction of $PtO_x$ species in interaction with $CeO_2$ and to the reduction of the superficial oxygen of $CeO_2$. This peak is shifted to a higher temperature in comparison with that of Pt/Ce probably because of the presence of aluminum. The $H_2$ uptake at 428 °C can be associated with the reduction of the dispersed Pt in isolated particles [50,54].

For the Pt/CeZr catalyst, the peaks corresponding to the reduction of Pt oxide and surface cerium oxide species are shifted to higher temperatures in comparison with the other ceria-based catalysts (337 °C). The second peak on the TPR profile of Pt/CeZr (517 °C) can be attributed to the reduction of superficial zirconium oxide species [55–57].

The TPR profile of the Pt/AlZr catalyst shows a broad peak, which has its maximum at ~813 °C and can be related to the reduction of the $PtO_x$ species.

### 3.1.5. OSC measurements

Fig. 4 shows the diagrams of the OSC of each platinum catalyst used as coating for the monolith. These values were measured at 400 °C.

These results show clearly the beneficial effect of the presence of cerium on the OSC values and are in accordance with the literature [58–60]. Actually, the platinum catalysts supported on $Al_2O_3$, $ZrO_2$, or $Al_2O_3$–$ZrO_2$ have low OSC values, which could be related to the contribution of the metal [61], whereas the catalysts containing cerium possess higher values of OSC. The higher OSC value of Pt/CeZr in comparison with that of Pt/Ce has been already encountered in the literature [58,60] and explained by the

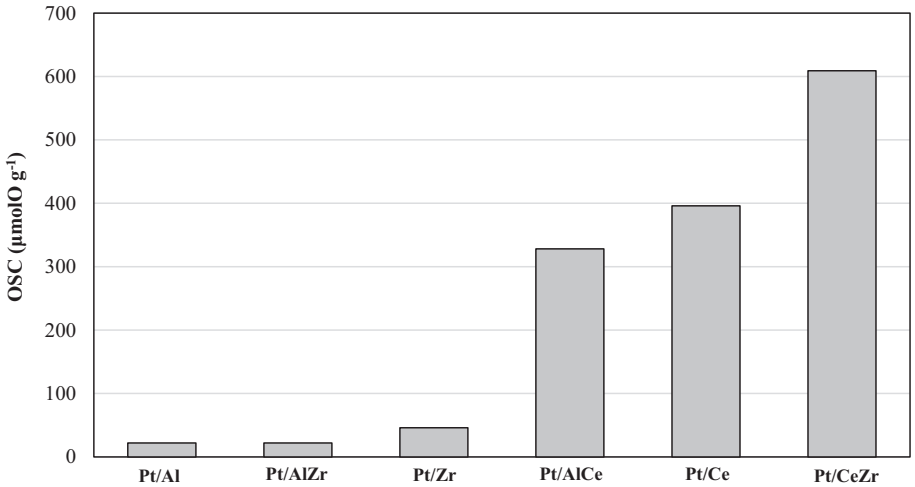


**Fig. 4.** OSC of the synthesized platinum catalysts measured at 400 °C.

**Table 3**
Global activities in 33DMB1 isomerization and $CO_2$ chemisorbed for each catalyst.

| Catalysts | $A_{33DMB1}$ ($\mu mol\ m^{-2}\ h^{-1}$) | $CO_2$ chemisorbed ($\mu mol\ m^{-2}$) |
|---|---|---|
| Pt/Al | 189 | 4 |
| Pt/AlZr | 94 | 17 |
| Pt/Zr | 38 | 80 |
| Pt/AlCe | 1.5 | 34 |
| Pt/Ce | 1.1 | 210 |
| Pt/CeZr | 0.7 | 136 |

defective structure due to the presence of $Zr^{4+}$ in the ceria lattice as shown earlier in XRD analysis (Fig. 2(c)).

The theoretical number of reducible surface oxygen atoms ($OSC_{surf}$), the OSC of metal ($OSC_{Pt}$), and the NLs involved in the storage process have been calculated and the results are reported in Table 2. The NL values show that bulk oxygen atoms are involved in the case of mixed oxides–supported platinum catalysts ($1 < NL < 3$), whereas oxygen storage is limited to the surface of Pt/Ce ($NL = 0.75$, Table 2). This result confirms that the introduction of Al or Zr cations greatly improve the redox process of the catalysts. The insertion of these additives into $CeO_2$ leading to the lattice deformation generates higher mobility of oxygen atoms [62].

*3.1.6. Evaluation of the Brønsted acidity and the basicity*

The model reaction of 33DMB1 isomerization was performed at 300 °C, and the $CO_2$ chemisorption was performed at room temperature for all catalysts. Table 3 presents the global activities in 33DMB1 isomerization and the $CO_2$ chemisorbed for each catalyst.

It is important to note that platinum has been proved to have no activity in 33DMB1 isomerization; however, the metal impregnation can induce changes in the surface acidity depending on the nature of the oxide [48]. In agreement with the literature, the alumina-supported platinum catalyst exhibits a higher acidity whereas the catalysts based on cerium oxides have very low activities in 33DMB1 isomerization. The presence of aluminum in the Pt/AlZr catalyst improves the acidity of the zirconia-supported platinum catalyst.

Contrary to the acidity, the Pt/Ce catalyst exhibits a higher basicity. This result is in accordance with the studies, which show that ceria is essentially basic [48,63]. The addition of cerium to aluminum and zirconium oxides increases the basicity of these latter. As presented by Martin and Duprez [48], Pt/Zr exhibits also a relatively high basicity. The addition of zirconium increases the initial basicity of Pt/Al. This effect has already been presented by Trejo et al. [63]. The low basicity of Pt/Al can be related to its surface hydroxyl groups.

*3.2. Catalytic tests*

The catalytic performances of the monolithic catalysts are presented in terms of $CO_2$ yield plots (Fig. 5), the temperatures of 10%, 50%, and 90% of acetic acid conversion (Table 4), and the specific activities (Table 5).

Before the evaluation of the catalytic performances of the monolithic platinum catalysts, catalytic tests were carried out on a bare monolith and on both monolithic and powder $Al_2O_3$–$CeO_2$ to investigate the effect of the monolith washcoating and of the catalyst shaping. On the bare monolith, a noticeable $CO_2$ yield can be observed from ~240 °C and an acetic acid conversion of 50% is obtained at 290 °C (Fig. 5 and Table 4). The washcoating of $Al_2O_3$–$CeO_2$ over the monolith leads to a shift of the conversion to lower temperatures. Actually, as shown in Table 4, when the washcoated $Al_2O_3$–$CeO_2$ catalyst is used instead of the bare monolith the $T_{10}$, $T_{50}$, and $T_{90}$ temperatures are lowered by 55, 52, and 57 °C, respectively. This result shows the contribution of the catalyst coating in terms of catalytic

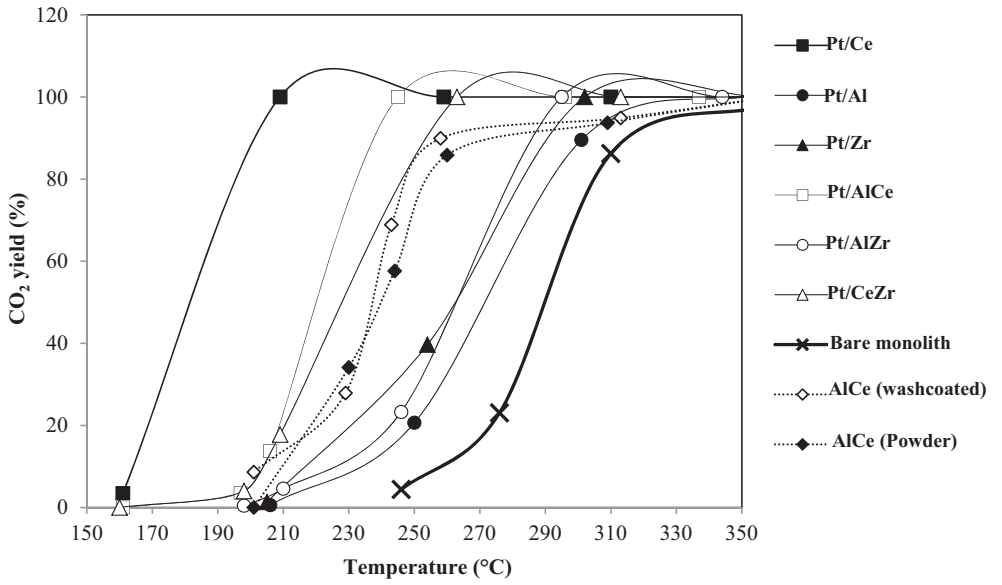


**Fig. 5.** Carbon dioxide formation during the acetic acid oxidation on the synthesized monolithic catalysts.

**Table 4**
$T_{10}$, $T_{50}$, and $T_{90}$ for the total oxidation of acid acetic.

| Catalysts | $T_{10}$ (°C) | $T_{50}$ (°C) | $T_{90}$ (°C) |
|---|---|---|---|
| Bare monolith | 260 | 290 | 317 |
| AlCe (washcoated) | 205 | 238 | 260 |
| AlCe (powder) | 210 | 240 | 274 |
| Pt/Ce | 165 | 184 | 202 |
| Pt/AlCe | 205 | 220 | 238 |
| Pt/CeZr | 205 | 228 | 252 |
| Pt/AlZr | 226 | 263 | 286 |
| Pt/Zr | 213 | 264 | 291 |
| Pt/Al | 233 | 272 | 302 |

activity. However, the catalyst shaping presents no significant changes in the catalytic performances. In fact, only a decrease of about 4 °C is observed when the test is performed on the washcoated sample instead of the $Al_2O_3$–$CeO_2$ powder (Table 4).

Among all the monolithic platinum catalysts, Pt/Ce is the catalyst, which exhibits a $CO_2$ appearance at lower temperatures (Fig. 5). In fact as shown in Table 4, at 202 °C the acetic acid conversion reaches 90% with Pt/Ce, whereas at this temperature the conversion is less than 10% with the others catalysts. Pt/Al is the monolithic platinum catalyst on which the acetic acid conversion occurs at the higher temperatures. The presence of ceria in the Pt/AlCe catalyst decreases significantly the conversion temperatures of Pt/Al. For example, $T_{50}$ is lowered by 52 °C as described in the previous work [64]. The same benefit is observed when zirconium oxide is added to aluminum oxide, even if, in this case the promotion is lower (Table 4). For Pt/Zr, the plot of $CO_2$ appearance is close to that obtained with Pt/AlZr (Fig. 5). The presence of ceria in the Pt/CeZr catalyst has the same promoting effect (compared to Pt/Zr) as its presence in Pt/AlCe (compared to Pt/Al). However, for higher conversions, $CO_2$ appears at lower temperatures with Pt/AlCe. Because the coated layer weight and the metal loading are different for each catalyst, the $CO_2$ yield plots are sufficient to compare their catalytic performances. Therefore, catalytic activities have been calculated per gram of metal (specific activity ($A_s$)), per square meter of catalyst, and per gram of coated layer (global activity (A)) and are reported in Table 5. These activities were calculated at different temperatures (165, 198, and 207 °C) so as to remain below 20% of acetic acid conversion. It can be remarked that generally activities increase together except the case of Pt/Z and Pt/AlZr catalysts. In fact Pt/Zr has a specific activity lower than that of Pt/AlZr (0.72 vs 0.86 mmol $h^{-1}$ $g^{-1}_{metal}$), whereas its global activity is higher (4.66 vs 3.69 μmol $h^{-1}$ $g^{-1}_{cat}$). Unsurprisingly, Pt/Ce appears to be the most active catalyst for the acetic acid oxidation whereas with Pt/AlCe the formation of $CO_2$ occurs at lower temperatures than with Pt/CeZr, the latter being more active than Pt/AlCe. Pt/Al is the less active catalyst for the acetic acid oxidation.

To explain the difference observed between the catalytic activities, the existence of any correlation between the global activity and the redox and acid–base properties has been checked. For the redox properties only the surface OSC ($OSC_{surf}$) has been considered. In fact, because the oxidation reaction occurs at low temperatures, the bulk oxygen storage could not be considered to be involved in the catalytic process. Fig. 6 shows the relation among $OSC_{surf}$, $A_{33DMB1}$, $CO_2$ chemisorbed, and *A* calculated at 165 (a), 198 (b), and 207 °C (c) expressed by a unit of catalyst surface area.

### 3.2.1. Relation between $OSC_{surf}$ and basicity

Generally, a good correlation exists between the catalysts basicity determined by carbon dioxide chemisorption and the OSC. Indeed, higher the OSC, higher is the basicity. Similar results are observed in previous works [48]. Nevertheless, an exception can be noted for the catalysts Pt/AlCe and Pt/Zr. In fact Pt/AlCe has a more important $OSC_{surf}$ than Pt/Z, which has a higher basicity.

### 3.2.2. Relation among $OSC_{surf}$, basicity, and global activity

Once again a good correlation is observed between the $OSC_{surf}$ values and the global activity values. Actually, the catalysts with the lowest $OSC_{surf}$ values are less active in the acetic acid oxidation. Moreover, higher the $OSC_{surf}$ value, higher is the global activity value. The OSC can therefore be considered as an important parameter that influences the catalytic activity.

Similarly, a good correlation can also be established between the basicity and the catalytic activity; higher the $CO_2$ chemisorbed value, higher is the global activity value. Acetic acid is a difficult molecule to adsorb. In some way it could be compared with $CO_2$. Lavalley [65] showed that $CO_2$ adsorption on the surface of metallic oxides generates different carbonate species. These carbonates characterize the basic strength of the catalyst. Weak sites are formed through hydroxy groups (OH) on the surface of the catalyst, whereas medium and strong sites are linked to the existence of $O^{2-}$ ions, whose coordination depends on the metal–oxygen $M^{n+}$–$O^{-}$ bond. As to $CeO_2$, its basicity is

**Table 5**
Specific activity and global activity of each catalyst at 165, 198, and 207 °C.

| Catalysts | Specific activity ($A_s$) (mmol $h^{-1}$ $g^{-1}_{metal}$) | | | Global activity (*A*) (μmol $h^{-1}$ $g^{-1}_{cat}$) | | | Global activity per square meter ($10^{-2}$ μmol $h^{-1}$ $m^{-2}$) | | |
|---|---|---|---|---|---|---|---|---|---|
| | 165 °C | 198 °C | 207 °C | 165 °C | 198 °C | 207 °C | 165 °C | 198 °C | 207 °C |
| Pt/Ce | 1.53 | – | – | 6.28 | – | – | 7.12 | – | – |
| Pt/CeZr | 0.13 | 1.2 | – | 0.64 | 5.89 | – | 0.85 | 7.90 | – |
| Pt/AlCe | 0.06 | 0.61 | – | 0.2 | 2.06 | – | 0.21 | 2.19 | – |
| Pt/AlZr | 0 | 0.13 | 0.86 | 0 | 0.54 | 3.69 | 0 | 0.63 | 4.34 |
| Pt/Zr | 0 | 0 | 0.72 | 0 | 0 | 4.66 | 0 | 0 | 35.3 |
| Pt/Al | 0 | 0 | 0.47 | 0 | 0 | 0.95 | 0 | 0 | 0.78 |

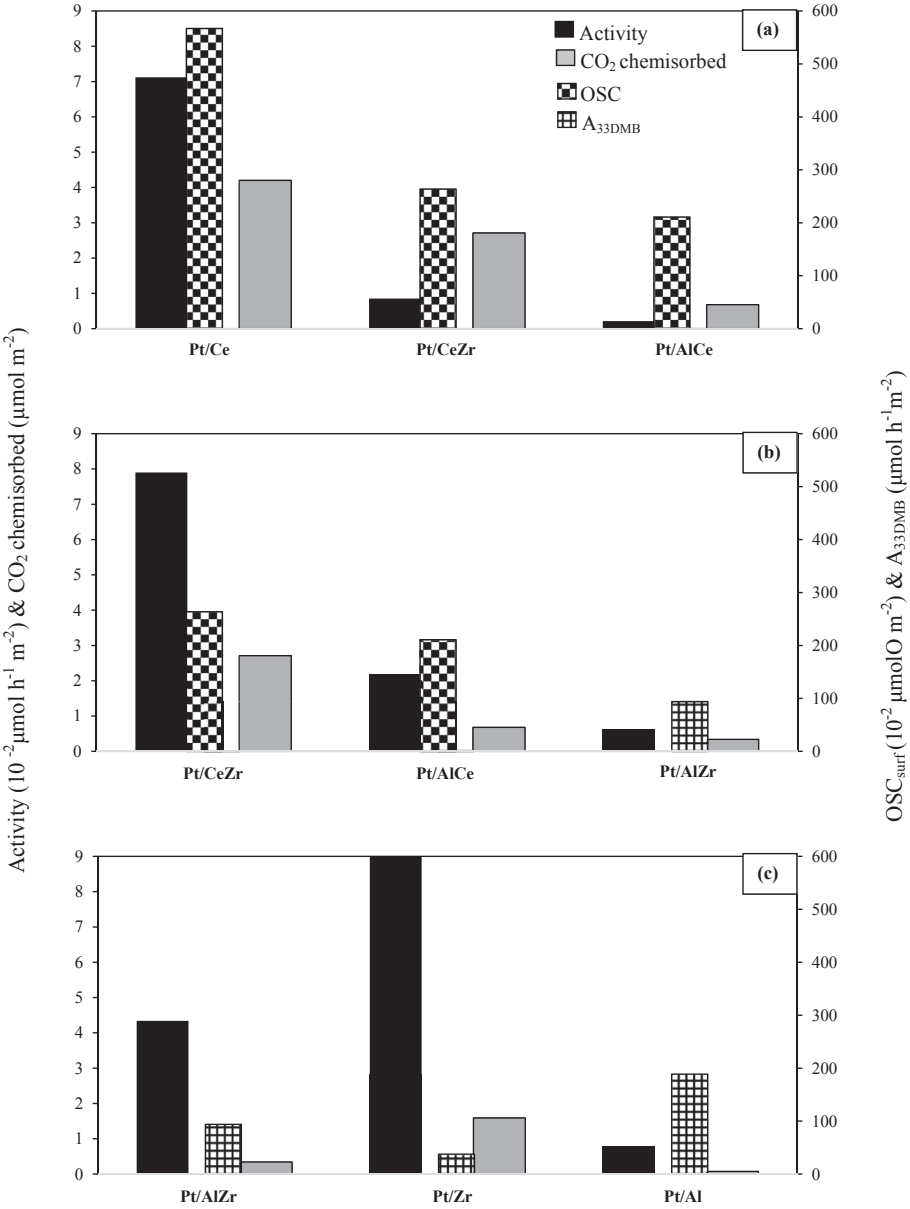


**Fig. 6.** Relation among OSC, acidity, basicity, and catalytic activity measured at (a) 165 °C, (b) 198 °C, and (c) 207 °C.

mainly because of medium and strong sites. Binet et al. [66] showed that the formation of carbonate species on the surface of ceria depends on the $M^{n+}$–$O^{-}$ bonds, which favor the formation of the medium and strong sites. The presence of these particular basic sites could explain the better activity of the ceria-based catalysts. Therefore, the catalysts should not be too basic as acetic acid may stay adsorbed on the surface and then not react. A good balance must be found. Melang Me Nze et al. [67] have compared two preparation methods and showed differences in the acid–base properties, leading to differences in activity. They also showed that the catalyst should not be too basic as an important formation of carbonate species on the surface of the catalyst would affect the activity of the catalysts. Nevertheless, an exception is observed for the catalysts Pt/AlCe and Pt/Zr. In fact Pt/AlCe is more active than Pt/Zr, although its basicity is lower than that of Pt/Zr (Fig. 6(b) and (c)). It is important to note that Pt/AlCe has an $OSC_{surf}$ value higher than that of Pt/Zr/M. This result confirms the conclusion emitted from the relation between the OSC and the global activity. The basic property of the catalyst affects the catalytic activity without being a sufficient parameter to predict the catalytic performances. Therefore, the high basicity of Pt/Ce coupled to its good OSC can explain the high catalytic activity of the latter. This observation agrees with the study previously published

[68], in which it has been proposed the abstraction of the proton acid of acetic acid by the catalyst basic sites as the limiting step of the oxidation. The mechanism of acetic acid oxidation formed intermediates such as acetone, methanol, and formaldehyde. The production of these molecules involves reducible Lewis acid sites ($Ce^{4+}$) and reactive Lewis base sites ($O^{2-}$) [68].

*3.2.3. Relation between Brønsted acidity and global activity*

It can be observed that higher the Brønsted acidity, lowest is the catalytic activity. Indeed, the catalysts with the lowest acidities are the most active, whereas the most acidic catalyst (Pt/Al) is less active (Fig. 6). Therefore, the Brønsted acidity seems to inhibit the catalytic activity for the acetic acid activity. The acidic nature of the VOCs could explain this effect of the catalyst acidic property.

## 4. Conclusion

Acetic acid oxidation was studied over monolithic catalysts coated with platinum-supported catalysts $Pt/Al_2O_3$, $Pt/ZrO_2$, $Pt/CeO_2$, $Pt/Al_2O_3$, $Pt/Al_2O_3–ZrO_2$, $Pt/Al_2O_3–CeO_2$, and $Pt/CeO_2–ZrO_2$. The washcoat process was influenced by the nature of the catalyst used to coat the cordierite monolith. Thus, on $Pt/CeO_2$ catalyst the layer coated was the highest, whereas the monolithic catalyst coated with $Pt/ZrO_2$ exhibits the lowest layer coated. The characterization of the catalysts showed that the catalysts containing ceria were the most basic and the most reducible. The redox and acid–base properties seem to influence the catalytic activity for the reaction of acetic acid oxidation. A correlation established among the OSC, the basicity, and the catalytic global activity has shown that

- generally the basicity correlates with the surface OSC except for the zirconia platinum–supported catalyst, which has no $OSC_{surf}$ but has a higher basicity;
- higher the $OSC_{surf}$, higher is the catalytic global activity;
- the more basic catalysts exhibit the highest catalytic activity except $Pt/ZrO_2$, which was less active than $Pt/Al_2O_3–CeO_2$ even if the latter has a lower basicity;
- the Brønsted acidity appears to inhibit the catalytic activity, thus the most acidic catalysts were those with the lowest catalytic activity.

On the basis of these correlations, we can say that the basicity is an important parameter for the reaction of acetic acid oxidation, but the OSC can be considered as the key factor of this reaction.

## References


[1] K.-H. Kim, S.O. Baek, Y.-J. Choi, Y. Sunwoo, E.-C. Jeon, J.H. Hong, Environ. Monit. Assess. 118 (2006) 407–422.
[2] N. Ali, C. Lu, R. Masel, Catal. Today 62 (2000) 347–353.
[3] E. Pagans, X. Font, A. Sánchez, J. Hazard. Mater. 131 (2006) 179–186.
[4] P. Hobbs, J. Webb, T. Mottram, B. Grant, T. Misselbrook, J. Sci. Food Agric. 84 (2004) 1414–1420.
[5] E. Zervas, M. Tazerout, Atmos. Environ. 34 (2000) 3921–3929.
[6] E. Rivière, CITEPA Report, Paris, 1998.
[7] H. Fontaine, M. Veillerot, J.C. Gallo, Proceedings of the 8th International Symposium on Transport and Air Pollution, 1999.
[8] L. Malherbe, C. Mandin, Atmos. Environ. 41 (2007) 6322–6330.
[9] H.-M. Liang, C.-M. Liao, Chemosphere 68 (2007) 781–789.
[10] K. Pirkanniemi, M. Sillanpää, Chemosphere 48 (2002) 1047–1060.
[11] E. Sanhueza, L. Figueroa, M. Santana, Joint 8th CAGCP and 2nd IGAC Conference on Global Atmosheric Chemistry, 30, 1996, pp. 1861–1873.
[12] E. Sanhueza, M.O. Andreae, Geophys. Res. Lett. 18 (1991) 1707–1710.
[13] D. Grosjean, Atmos. Environ. 26 (1992) 3279–3286.
[14] S. Ojala, S. Pitkäaho, T. Laitinen, N.N. Koivikko, R. Brahmi, J. Gaálová, L. Matejova, A. Kucherov, S. Päivärinta, C. Hirschmann, T. Nevanperä, M. Riihimäki, M. Pirilä, R.L. Keiski, Top. Catal. 54 (2011) 1224–1256.
[15] P. Le Cloirec, Les Composés Organiques Volatils (COV) dans l'Environnement, Tech. & Doc., Lavoisier, Paris, 1998, 737 p, ISBN 2-7430-0232-8.
[16] L. Oliviero, J. Barbier Jr., D. Duprez, H. Wahyu, J.W. Ponton, I.S. Metcalfe, D. Mantzavinos, Appl. Catal., B 35 (2001) 1–12.
[17] J. Levec, A. Pintar, Catal. Today 24 (1995) 51–58.
[18] J. Tsou, P. Magnoux, M. Guisnet, J.J.M. Órfão, J.L. Figueiredo, Appl. Catal., B 57 (2005) 117–123.
[19] R. López-Fonseca, B. de Rivas, J.I. Gutiérrez-Ortiz, A. Aranzabal, J.R. González-Velasco, Appl. Catal., B, 3rd International Conference on Environmental Catalalysis 41 (2003) 31–42.
[20] H.L. Tidahy, S. Siffert, J.-F. Lamonier, R. Cousin, E.A. Zhilinskaya, A. Aboukaïs, B.-L. Su, X. Canet, G. De Weireld, M. Frère, J.-M. Giraudon, G. Leclercq, Paper Presented at the 4th International Conference on Environment Catalysis. 4th ICEC Heidelberg, Germany, June 05–08 2005, 70, 2007, pp. 377–383.
[21] M. Gallastegi-Villa, M. Romero-Sáez, A. Aranzabal, J.A. González-Marcos, J.R. González-Velasco, Catal. Today 213 (2013) 192–197.
[22] M. Baldi, E. Finocchio, F. Milella, G. Busca, Appl. Catal., B 16 (1998) 43–51.
[23] S. Hamoudi, K. Belkacemi, F. Larachi, Chem. Eng. Sci. 54 (1999) 3569–3576.
[24] L.F. Liotta, M. Ousmane, G. Di Carlo, G. Pantaleo, G. Deganello, G. Marcì, L. Retailleau, A. Giroir-Fendler, Appl. Catal., A 347 (2008) 81–88.
[25] V.H. Vu, J. Belkouch, A. Ould-Dris, B. Taouk, J. Hazard. Mater. 169 (2009) 758–765.
[26] W. Xingyi, K. Qian, L. Dao, Appl. Catal., B 86 (2009) 166–175.
[27] P. Papaefthimiou, T. Ioannides, X.E. Verykios, Appl. Catal., B 13 (1997) 175–184.
[28] C. Lahousse, A. Bernier, P. Grange, B. Delmon, P. Papaefthimiou, T. Ioannides, X. Verykios, J. Catal. 178 (1998) 214–225.
[29] P. Papaefthimiou, T. Ioannides, X.E. Verykios, Catal. Today 54 (1999) 81–92.
[30] V.P. Santos, S.A.C. Carabineiro, P.B. Tavares, M.F.R. Pereira, J.J.M. Órfão, J.L. Figueiredo, Appl. Catal., B 99 (2010) 198–205.
[31] Z. Abbasi, M. Haghighi, E. Fatehifar, S. Saedy, J. Hazard. Mater. 186 (2011) 1445–1454.
[32] S. Scirè, L.F. Liotta, Appl. Catal., B 125 (2012) 222–246.
[33] P. Rodriguez, F. Simescu-Lazar, V. Meille, T. Bah, S. Pallier, I. Fournel, Appl. Catal., A 427–428 (2012) 66–72.
[34] A.A. Klinghoffer, R.L. Cerro, M.A. Abraham, Catal. Today 40 (1998) 59–71.
[35] R. Brahmi, Y. Batonneau, C. Kappenstein, P. Miotti, M. Tajmar, C. Scharlemann, M. Lang, in: E.M. Gaigneaux (Ed.), Studies in Surface Science and Catalysis, vol. 162, Elsevier, Amsterdam, 2006, pp. 649–656.
[36] G. Groppi, E. Tronconi, Chem. Eng. Sci. 55 (2000) 2161–2171.
[37] D. Amariei, R. Amrousse, Y. Batonneau, R. Brahmi, C. Kappenstein, B. Cartoixa, in: E.M. Gaigneaux (Ed.), Studies in Surface Science and Catalysis, vol. 175, Elsevier, Amsterdam, 2010, pp. 35–42.
[38] F. Simescu-Lazar, V. Meille, S. Pallier, E. Chaînet, C. De Bellefon, Appl. Catal., A 453 (2013) 28–33.
[39] S. Azalim, R. Brahmi, M. Agunaou, A. Beaurain, J.-M. Giraudon, J.-F. Lamonier, Chem. Eng. J. 223 (2013) 536–546.
[40] R.M. Heck, S. Gulati, R.J. Farrauto, Chem. Eng. J. 82 (2001) 149–156.
[41] X. Xiaoding, H. Vonk, A. Cybulski, J.A. Moulijn, in: G. Poncelet (Ed.), Studies in Surface Science and Catalysis, vol. 91, Elsevier, Amsterdam, 1995, pp. 1069–1078.
[42] H. Pérez, P. Navarro, M. Montes, Chem. Eng. J. 158 (2010) 325–332.
[43] D. Duprez, J. Chim. Phys. Phys. Chim. Biol. 80 (1983) 487–505.
[44] J. Mikulová, J. Barbier Jr., S. Rossignol, D. Mesnard, D. Duprez, C. Kappenstein, J. Catal. 251 (2007) 172–181.
[45] S. Kacimi, J. Barbier, R. Taha, D. Duprez, Catal. Lett. 22 (1993) 343–350.
[46] S. Rossignol, Y. Madier, D. Duprez, Catal. Today 50 (1999) 261–270.
[47] H. Pines, J. Catal. 78 (1982) 1–16.
[48] D. Martin, D. Duprez, J. Mol. Catal. Chem. 118 (1997) 113–128.
[49] M. Yue, M. Cui, N. Zhang, Z. Long, X. Huang, J. Rare Earths 31 (2013) 251–256.
[50] S. Damyanova, J.M. Bueno, Appl. Catal., A 253 (2003) 135–150.

[51] H. Lieske, G. Lietz, H. Spindler, J. Völter, J. Catal. 81 (1983) 8–16.
[52] J.Z. Shyu, K. Otto, J. Catal. 115 (1989) 16–23.
[53] A.C.S.F. Santos, S. Damyanova, G.N.R. Teixeira, L.V. Mattos, F.B. Noronha, F.B. Passos, J.M.C. Bueno, Appl. Catal., A 290 (2005) 123–132.
[54] M.J. Tiernan, O.E. Finlayson, Appl. Catal., B 19 (1998) 23–35.
[55] S. Damyanova, B. Pawelec, K. Arishtirova, M.V.M. Huerta, J.L.G. Fierro, Appl. Catal., B 89 (2009) 149–159.
[56] R. Pérez-Hernández, F. Aguilar, A. Gómez-Cortés, G. Díaz, Sel. Contrib. XIX Ibero Am. Catal. Symp. Sel. Contrib. XIX Ibero Am. Catal. Symp. 107–108 (2005) 175–180.
[57] L. Mattos, E. de Oliveira, P. Resende, F. Noronha, F. Passos, Catal. Today 77 (2002) 245–256.
[58] J. Mikulová, S. Rossignol, J. Barbier Jr., D. Duprez, C. Kappenstein, Catal. Today 124 (2007) 185–190.
[59] J. Fonseca, S. Royer, N. Bion, L. Pirault-Roy, M. do C. Rangel, D. Duprez, F. Epron, Appl. Catal., B 128 (2012) 10–20.
[60] J. Mikulová, S. Rossignol, J. Barbier Jr., D. Mesnard, C. Kappenstein, D. Duprez, Appl. Catal., B 72 (2007) 1–10.
[61] S. Bedrane, C. Descorme, D. Duprez, Catal. Today 75 (2002) 401–405.
[62] G. Vlaic, P. Fornasiero, S. Geremia, J. Kašpar, M. Graziani, J. Catal. 168 (1997) 386–392.
[63] F. Trejo, M.S. Rana, J. Ancheyta, A. Rueda, ISAHOF2011 “Feed and Processes for the Production of Clean Fuels” 100 (2012) 163–172.
[64] J.C. Lavalley, Trends Phys. Chem. 2 (1991) 305–327.
[65] J.C. Lavalley, Catal. Today 27 (1996) 377–401.
[66] C. Binet, M. Daturi, J.C. Lavalley, Catal. Today 50 (1999) 207–225.
[67] V. Melang Me Nze, C. Fontaine, J. Barbier Jr., C. R. Chimie 20 (2017) 67–77.
[68] H.-J. Sedjame, C. Fontaine, G. Lafaye, J. Barbier Jr., Appl. Catal., B 144 (2014) 233–242.